Flow, Turbulence and Combustion (2026) 116:27
https://doi.org/10.1007/s10494-025-00727-7

RESEARCH

Prediction of Laminar Separation Bubble on Airfoils at Low Reynolds Number

Carlo Brunelli[1,2,3] · Matija Avirovic[1,3,4] · Bart Janssens[1] · Benoît G. Marinus[1] · Koen Hillewaert[3,5] · Mark Runacres[2]

Received: 4 June 2025 / Accepted: 18 December 2025

Abstract
The accurate prediction of Laminar Separation Bubbles (LSBs) is crucial for understanding transition mechanisms and aerodynamic performance of airfoils operating at low Reynolds numbers. This study employs the Linearized and Segregated Variational Multiscale (VMS) Method to simulate LSB formation and development on airfoils. The methodology is validated against two well-documented test cases: SD7003 airfoil $\boldsymbol{Re} = 60\,000$, $\boldsymbol{AoA} = 4^\circ$ and the E387 airfoil at $\boldsymbol{Re} = 3 \times 10^5$, $\boldsymbol{AoA} = 1^\circ$. The results demonstrate strong agreement with reference data from the literature, accurately capturing pressure and skin friction distributions as well as velocity profiles associated with LSB dynamics. To further assess the method's predictive capability, simulations are performed on a DU89-134 airfoil, designed for High Altitude Pseudo Satellites (HAPS) applications at $\boldsymbol{Re} = 5 \times 10^5$, $\boldsymbol{AoA} = 1^\circ$, 5°. Comparisons with experimental vertical velocity profiles - obtained with hot-wires anemometry - show excellent agreement, confirming the method's robustness in transitional flow modelling. These findings highlight the effectiveness of the Linearized and Segregated VMS approach for Large Eddy Simulations of LSBs. The method provides a reliable tool for aerodynamic analysis of low-Reynolds-number airfoils, with potential applications in next-generation high-altitude flight vehicles.

Keywords Laminar separation bubble · Variational multiscale method · Implicit LES

1 Introduction

Over the last decade, low-Reynolds number flows have attracted significant attention, especially in the context of emerging High-Altitude Pseudo-Satellites (HAPS) and other aerospace applications. Operating at low Reynolds numbers - in the range $10^4 - 10^6$ (García-Gutiérrez et al. 2020) - these vehicles present unique aerodynamic phenomena and engineering challenges. HAPS usually operate in the stratosphere at altitudes between 17 and 22 km and serve as innovative devices for various purposes, including surveillance, telecommunications, and environmental monitoring. They fly at altitudes with low air density and low cruise speeds. These two elements combined with a small chord result in a

Extended author information available on the last page of the article

Published online: 08 January 2026

low-Reynolds number regime. In these conditions, the operating Reynolds number lies within the range where the transition from laminar to turbulent flow has strong implications for airfoil performance, and viscous forces become significant in determining the flow's characteristics. Laminar boundary layers can separate so the Laminar Separation Bubble (LSB) forms as long as flow does not transition upstream of separation. LSBs are regions of reversed flow on an airfoil's surface that can severely affect lift, drag, and overall aerodynamic performance. Accurately predicting the formation of LSB is essential for maintaining the efficiency and stability of operational vehicles. At high altitudes, the harsh environment makes in-flight experiments testing particularly challenging. Wind tunnel testing facilities with low speeds and low turbulence levels are required for meaningful experiments. Therefore, reliable numerical methods are indispensable for simulating and predicting performance. In this context, airfoils like the DU89-134 (Boermans and Garrel 1997), originally designed for sailplanes, are an example of designs engineered to achieve a high lift-to-drag ratio required for prolonged high-altitude missions. Currently, different methods are available to study low-Reynolds airfoils flows including two-dimensional laminar simulations (Lee et al. 2017), and RANS simulations with $k-\omega\ SST$ turbulence model coupled with transition models (Carreño Ruiz and D'Ambrosio 2022; Windte et al. 2006; Mourousias et al. 2023), LES (Wiart and Hillewaert 2012; Garmann et al. 2013), wall-resolved LES (wrLES) (Frère et al. 2018), implicit LES (iLES) using Galerkin based methods (Uranga et al. 2011; Beck et al. 2014). On the other hand, 2-D simulations have moderate computational cost, but they can be used to evaluate only qualitatively the aerodynamic characteristics for low angle of attack, (Lee et al. 2017; Windte et al. 2006; Gunel et al. 2016; Morgado et al. 2016). 2-D simulations also lead to spurious effects in the pressure distribution where the LSB develops (Koning et al. 2023).

In the context of iLES, a Linearized and Segregated version of the original Variational MultiScale Method (LS-VMS), has been used in (Brunelli et al. 2025) to study passive flow control on the DU89-134 airfoil. Traditional LES models typically rely on explicit subgrid-scale (SGS) models-such as Smagorinsky or dynamic models-to approximate the effect of unresolved turbulence. These models often require heuristic assumptions, and tuning parameters (Sagaut 2006). In contrast, the VMS introduces a mathematically consistent separation of resolved and unresolved scales within the finite element formulation (Hughes et al. 2000). This built-in scale separation naturally leads to residual-based modeling of the subgrid scales, avoiding ad hoc turbulence models and allowing the method to act as an implicit LES (iLES). As a result, VMS provides improved robustness and accuracy, especially in transitional and wall-bounded flows, and offers a unified framework for stabilization and turbulence modeling (Bazilevs et al. 2007).

The present research intends to provide additional detailed insights into the applicability, numerical accuracy and robustness of LS-VMS for aerodynamic analysis of airfoils designed for HAPS, demonstrating its capability in predicting transition mechanisms, focusing on the prediction of the LSB, in high-altitude flight conditions. In this paper, the LS-VMS approach for airfoils at low Reynolds numbers is successfully validated using the standard case of the SD7003 and E387 airfoils. The research aims to compare the results obtained with the $k-\omega\ SST$ turbulence model coupled with the $\gamma - Re_\theta$ transition model, wind tunnel experiments, and the LS-VMS. The comparison includes data from infrared thermography and hot-wire analysis, in addition to RANS modeling, establishing the validity of the method for airfoils designed for HAPS applications. To further assess the robustness

of the LS-VMS method for low-Reynolds-number airfoils, a detailed analysis is performed, including grid and time-step dependence studies. Additionally, the turbulent kinetic energy spectra, obtained at various chordwise locations on the suction side of the DU89-134 airfoil.

2 LS-VMS Numerical Model

The three-dimensional unsteady incompressible flow above the aerofoil is solved using the LS-VMS method. This scheme is a linearized and segregated version of the variational multiscale (VMS) method, originally formulated in the two-scale (Hughes 1995; Hughes et al. 1998) and later extended to a three-scale framework particularly aimed at Large Eddy simulation of turbulent flows (Hughes et al. 2000). The LS-VMS implementation employed here was first presented in (Brunelli et al. 2024) and is openly available as a software package described in (Brunelli 2025). It has already been applied to study, for example, the effects of passive flow control devices on low-Reynolds-number airfoils (Brunelli et al. 2025, 2024). For a comprehensive overview of the different variants and developments within the VMS framework, we refer the reader to the recent reviews (Rasthofer and Gravemeier 2018; Ahmed et al. 2017).

The linearization technique improves computational efficiency by avoiding the need to solve a non-linear system at each time step and enabling independent solutions for the velocity and pressure systems. The VMS method can be catalogued as an implicit LES method and is based on the principle of scale separation between resolved and unresolved scales. We consider the following notation: $\mathbf{u}$ is the velocity, p the kinematic pressure, ν the kinematic viscosity, and f the volume force. The weak form of the Navier-Stokes equations is given by:

$$\begin{aligned} B_G = &\int_\Omega \frac{\partial \mathbf{u}}{\partial t} \cdot \mathbf{v}\, \mathbf{d\Omega} + \int_{\mathbf{\Omega}} (\mathbf{u} \cdot \nabla)\mathbf{u} \cdot \mathbf{v}\, \mathbf{d\Omega} + \int_{\mathbf{\Omega}} \nabla \mathbf{p} \cdot \mathbf{v}\, \mathbf{d\Omega} \\ &+ \int_\Omega \nu \nabla \mathbf{u} \cdot \nabla \mathbf{v}\, \mathbf{d\Omega} - \int_{\mathbf{\Omega}} \mathbf{f} \cdot \mathbf{v}\, \mathbf{d\Omega} + \int_{\mathbf{\Omega}} \mathbf{q}(\nabla \cdot \mathbf{u})\, \mathbf{d\Omega} = \mathbf{0} \end{aligned} \tag{1}$$

where $\mathbf{v} \in \mathbf{V}$ and $q \in Q$ are test functions for velocity and pressure; $V = \{\vec{v}\colon \Omega \to \mathbb{R}^3 | \vec{v}$ is a continuous over $\Omega\}$ for a 3D simualtion, and $Q = \{q\colon \Omega \to \mathbb{R} | q$ is a continuous over $\Omega\}$

The VMS method introduces new terms to the formulation and they contain the residuals of the continuity and momentum equations:

$$R_c = \nabla \cdot \mathbf{u} \tag{2}$$

$$\mathbf{R_m} = \frac{\partial \mathbf{u}}{\partial \mathbf{t}} + (\mathbf{u} \cdot \nabla)\mathbf{u} + \nabla \mathbf{p} - \nu \mathbf{\Delta u} - \mathbf{f} \tag{3}$$

The first set of terms are classical residual-based stabilization: Streamline Upwind Petrov-Galerkin (SUPG), Pressure-Stabilizing Petrov-Galerkin (PSPG), and Least-Squares Incompressibility Constraint (LSIC) (Hughes et al. 1986; Franca and Hughes 1988). From this viewpoint, classical stabilization methods serve as an intermediate step toward the comprehensive framework of VMS.

$$B_{\text{stab}} = \underbrace{\int_{\Omega} \tau_m \left(\mathbf{u}\cdot\nabla\mathbf{v}\right)\cdot\mathbf{R_m}\,\mathbf{d\Omega}}_{\textbf{SUPG}} + \underbrace{\int_{\Omega} \tau_m \left(\nabla q\right)\cdot\mathbf{R_m}\,\mathbf{d\Omega}}_{\textbf{PSPG}} + \underbrace{\int_{\Omega} \tau_c \left(\nabla\cdot\mathbf{v}\right)\mathbf{R_c}\,\mathbf{d\Omega}}_{\textbf{LSIC}} \tag{4}$$

where τ_m and τ_c are stabilization parameters defined as:

$$\tau_m = \left(\frac{4}{\Delta t^2} + \mathbf{u}\cdot\mathbf{G}\mathbf{u} + \mathbf{C_I}\nu^2\mathbf{G}:\mathbf{G}\right)^{-1/2} \tag{5}$$

$$\tau_c = \left(\tau_c \mathbf{g}\cdot\mathbf{g}\right)^{-1} \tag{6}$$

and Δt is the time-step, C_I is a positive constant, independent of the mesh size (John 2016). In all the cases presented $C_I = 36$ as used in (Evans et al. 2020; Janssens 2014; Trofimova et al. 2009). $\mathbf{G}$ and $\mathbf{g}$ depend on the local element size and orientation, more detail in (Bazilevs et al. 2007). The additional terms produced by the VMS introduce additional scale-separating effects, ensuring that unresolved scales contribute effectively to turbulence modelling, making it a more generalized and physically motivated approach compared to classical stabilization methods.

$$B_{VMS1} = \int_{\Omega} \left(\mathbf{u}\cdot\nabla\mathbf{v^T}\right)\cdot\left(\tau_\mathbf{m}\mathbf{R_m}\right)\mathbf{d\Omega} \tag{7}$$

$$B_{VMS2} = -\int_{\Omega} \left(\nabla\mathbf{v}\odot\tau_\mathbf{m}\mathbf{R_m}\otimes\tau_\mathbf{m}\mathbf{R_m}\right)\,d\Omega \tag{8}$$

The final stabilized equation is:

$$B_G + B_{stab} + B_{VMS1} + B_{VMS2} = 0 \tag{9}$$

The non-linear term $\mathbf{u}\cdot(\nabla\mathbf{u})$ can be linearized as $\mathbf{u_{adv}}\cdot(\nabla\mathbf{u})$, where $\mathbf{u_{adv}}$ is an approximation approximation of the velocity field, in the present method, the velocity field at the previous time-step.

The original VMS formulation involves solving a fully coupled system for velocity and pressure, which can be computationally expensive due to the nonlinear nature of the equations and the large system size (Bazilevs et al. 2007). To reduce this cost, LS-VMS approach decouples the velocity and pressure fields, allowing for their independent resolution - iteratively - within each time step. This results in a sequence of smaller, more efficient linear systems rather than a single large nonlinear system.

For an incompressible flow governed by the Navier-Stokes equations, the semi-discrete form after applying time integration using the θ-method (with θ=0.5, corresponding to the Crank-Nicolson scheme).

$$T\frac{\boldsymbol{x}^{n+1}-\boldsymbol{x}^n}{\Delta t} = -(A\boldsymbol{x}^{n+1}\theta + A\boldsymbol{x}^n(1-\theta)),$$

where: $\boldsymbol{x}$ represents the unknowns (velocity or pressure fields), T is the matrix accounting for time-dependent terms, A is the matrix incorporating spatial operators.

$$T_u \frac{\boldsymbol{u}^{n+1} - \boldsymbol{u}^n}{\Delta t} = -\theta A_u \boldsymbol{u}^{n+1} - (1-\theta) A_u \boldsymbol{u}^n + A_{up} p^n + \boldsymbol{f}_u, \tag{11}$$

$$T_p \frac{p^{n+1} - p^n}{\Delta t} = -\theta A_p p^{n+1} - (1-\theta) A_p p^n + A_{pu} \boldsymbol{u}^{n+1} + \boldsymbol{f}_p. \tag{12}$$

This formulation ensures that each sub-system is smaller enabling more efficient iterative solvers while maintaining accuracy. The decoupling of velocity and pressure provides significant computational savings compared to the monolithic approach (Brooks and Hughes 1982).

The LS-VMS formulation employed here was previously presented in (Brunelli 2025), where the method and its implementation were described. In (Brunelli 2025) three-dimensional Taylor-Green vortex (TGV3D) is used as a benchmark to assess discretization and time-integration errors.

However, the primary focus of this work is not on computational efficiency, but rather on assessing the applicability of the method for the accurate prediction of the LSB, an area where VMS-based approaches have been comparatively less explored.

3 VMS Set-Up

The method has been tested on three different airfoils: the SD7003, the E387, and the DU89-134. The SD7003 airfoil, from (Selig et al. 1989), at $Re = 60\,000$ and $AoA = 4°$ is an obvious choice due to its popularity in studying the formation of the LSB (Wiart and Hillewaert 2012), (Calderer and Masud 2013; Schmidt and Breuer 2017; Galbraith et al. 2008; Ol et al. 2012). The DU89-134, introduced in (Boermans and Garrel 1997), is a high L/D airfoil. It was originally designed for sailplanes while today it is used for HAPS applications. For this airfoil, the simulations are performed at Reynolds number of $Re = 500\,000$, with an angle of attack 1° and 5°. We are using an incompressible model, kinematic viscosity is calculated from Reynolds $\nu = (U_\infty c)/Re$. The time step Δt is non-dimensionalized using the flow-through time ($ftt = c/U_\infty$). It is fixed at $\Delta t/ftt = 1.0 \times 10^{-3}$ for the case at Reynolds number 60 000, and at $\Delta t/ftt = 5.0 \times 10^{-4}$ when the Reynolds number is $Re = 500\,000$. For studying the LSB at Re 60 000 over the airfoil SD7003 (Calderer and Masud 2013) use a time step of $\Delta t/ftt = 2.5 \times 10^{-3}$, Schmidt and Breuer (Schmidt and Breuer 2017) use $\Delta t/ftt = 3.0 \times 10^{-4}$, and both are using an airfoil with unitary chord length. Employing a time step of $\Delta t/ftt = 5.0 \times 10^{-4}$, 2000 time-steps are needed for one flow-over.

The domain dimensions are a trade-off between simulating far-field conditions and consequently not altering the flow past the airfoil, and having limited computational resources, which means having a feasible number of cells. VMS and RANS simulations are performed on a C-type domain with the same dimensions. The domain extends for 6c in front and 6c behind the airfoil, and is extruded by 0.2c (for the SD7003 airfoil analysis) in the spanwise direction, Fig. 1. The dimensions of the fluid domain are the same as the one used by (Calderer and Masud 2013) who tested the 2-scale VMS on the SD7003 at Reynolds 60 000

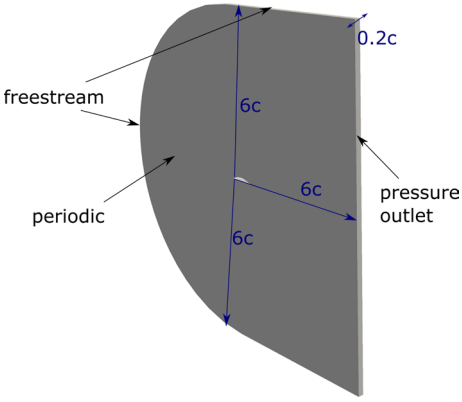

Fig. 1 Airfoil domain scheme

and 4°. Other authors proposed different domain sizes, see Table 1 for a comparison. (Kenji Takizawa and Tezduyar 2013) fixed the upper and lower boundaries of the mesh at 5c, the farfield at 10.5c from the midpoint of the airfoil together with an extension in the span direction of 0.1c for applying the Space-Time VMS. However, they studied near-stall conditions up to 18° and at a Reynolds number of 3×10^6. In (Frère et al. 2018) and (Schmidt et al. 2012), wrLES are performed at Reynolds number 1.64×10^6, and the extensions in the span direction are much lower, respectively: 0.01c and 0.05c.

No turbulence is introduced at the inlet, as done in (Wiart and Hillewaert 2012; Garmann et al. 2013; Frère et al. 2018). The far-field consists of a uniform inflow velocity $[U_\infty, 0, 0]$ prescribed on the outer boundary. The geometry and the 2D grid were created using Gmsh (Geuzaine and Remacle 2009). The 2D grid consists of a C-type mesh, see the mesh in Fig. 2. The 2D mesh is extruded and divided into 22 layers to obtain the 3D mesh. On the airfoil, a wall-normal mesh growth rate of about 1.12 is used. The wall-refinement in the streamwise (Δx^+), normal (Δy^+) and spanwise (Δz^+) directions are presented in Fig. 3, they are computed using in each point the time-averaged friction velocity u_τ. These refinements agree with Choi and Moin's guidelines (Choi and Moin 2012): i.e. $\Delta x^+ \approx 50 - 130$, $\Delta y^+ \approx 1$, $\Delta z^+ \approx 15 - 30$. These conditions apply to a fully developed boundary layer in the presence of a zero-pressure gradient and should be considered as general guidelines. They are followed as a widely accepted reference for wall-resolved LES resolution requirements, similarly as in (Frère et al. 2018). The spatial resolutions employed in the simulations for all three airfoils, are summarized in Table 2. We rely on the comparison between experiments and numerical results to actually ensure that transition is captured. Furthermore, at the leading edge, near the stagnation point, a singularity occurs. Increasing the resolution in this region amplifies the peak observed in Fig. 3, making it impossible to strictly satisfy these conditions there. The simulation ends after 20 *ftt*, corresponding to 4×10^5 time steps. Time-average is performed between $10ftt$ and $20ftt$, along with an averaging in the z direction.

3.1 Computational Cost Considerations

Direct Numerical Simulation (DNS) provides an essentially modelling-free numerical reference. However, its computational cost is prohibitive at the Reynolds numbers considered here, in particular at $Re = \mathcal{O}(10^5)$. The number of grid points required for DNS of wall-

Table 1 C-mesh domain dimension and time-step comparison for LES simulations

Author	half-circle radius [c]	farfield behind the airfoil [c]	spanwise [c]	Airfoil	$\Delta t/ftt$	Reynolds
Present research	6	6	0.2	SD7003	1.0×10^{-3}	6×10^4
Present research	6	6	-	E387	1.0×10^{-3}	3×10^5
Present research	6	6	0.05	DU89-134	5.0×10^{-4}	5×10^5
Calderer and Masud (2013)	6	6	0.2	SD7003	2.5×10^{-3}	6×10^4
Schmidt and Breuer (2017)	7	5	0.25	SD7003	3.0×10^{-4}	6×10^4
Kenji Takizawa and Tezduya (2013)	5	10.5	0.1	NACA 64–618	3.0×10^{-3}	3×10^6
Frére et al. (2018)	10	10	0.01	NACA4412	2.2×10^{-4}	1.64×10^6

bounded turbulence scales approximately as $Re^{9/4}$ (Choi and Moin 2012), while the total cost, including time stepping, grows even faster, typically as Re^3 (Piomelli 2008).

For illustration, (Wiart and Hillewaert 2012) reported that DNS of the SD7003 airfoil at $Re = 6 \times 10^4$ required roughly ten times the resolution of their corresponding LES (see their Table 1). The DNS of the NACA4412 airfoil at $Re = 4 \times 10^5$ by (Hosseini et al. 2016) employed nearly two orders of magnitude more grid points than the meshes used in the present LS-VMS simulations, far exceeding our available computational resources. These examples highlight that DNS is not a viable option for our target Reynolds number and geometric configuration.

4 RANS Set-Up

The RANS simulations are performed using STARCCM+ and are computed at the same Reynolds numbers and angles of attack as for the VMS. The fundamental difference between the two numerical solutions is the method. STARCCM+ solves the problem using the steady $k - \omega - SST$ model coupled with the $\gamma - Re\theta$ transitional model. Different calibrations are available (Suluksna et al. 2009; Langtry et al. 2006), by default (Suluksna et al. 2009) is used. In (Carreño Ruiz and D'Ambrosio 2022) has been pointed out that the coefficient s_1 can play a key role in determining the reattachment point, so different values are tested (s_1=2 and s_1=6).

The method requires a field function called *free-stream-edge-function*. It defines where the boundary layer is, with a value of 0 inside the boundary layer and a value of 1 outside, in the free stream. However, it is not easy to precisely know the thickness of the boundary-layer, δ_{99}, before running the simulation. A good estimation for turbulent boundary layer height it is provided by Eq. (13) as suggested by (Schlichting and Gersten 2016).

$$\delta_{99} = 0.37 \frac{x}{Re_x^{1/5}} \tag{13}$$

It is worth noting that the correlation (13) is derived for fully turbulent, zero-pressure-gradient flat-plate boundary layers. It is used as a practical estimate of the boundary-layer thickness for communication with the RANS solver. Since a turbulent boundary layer is always thicker than a laminar one at the same Reynolds number and streamwise location, this correlation provides a conservative upper bound.

Regarding the freestream value of turbulence intensity, (Schlichting and Gersten 2016) suggest that, based on experimental evidence, the effect for Turbulence Intensity $TI < 0.1\%$ is insignificant. On the other hand, (Langtry et al. 2006) sets $TI = 0.027\%$ as the minimum for numerical stability. Consequently, selecting $0.027\% \leq TI \leq 0.1\%$ at freestream appears to be a sensible option for comparisons with LES simulations that use an ideal freestream to reduce computational costs. Following the decision taken by (Carreño Ruiz and D'Ambrosio 2022), the simulations use a freestream turbulence intensity of 0.03%. At the inlet and outlet, turbulence intensity is set equal to 0.03%, to ensure numerical stability, as is also done by (Carreño Ruiz and D'Ambrosio 2022).

To capture the LSB in RANS simulations, it is necessary to employ a dense mesh with a minimum of 100 divisions along the airfoil chord and a first cell height that allows for a

Fig. 2 Mesh airfoil DU89-134

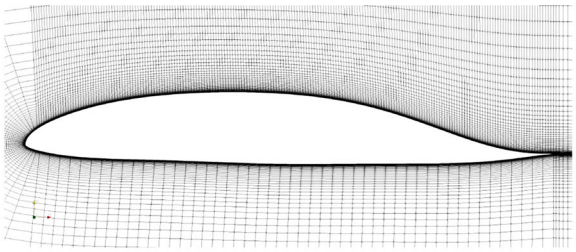

(a) Structured mesh around DU89

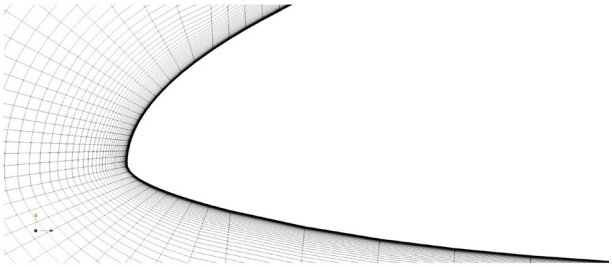

(b) Leading edge mesh detail

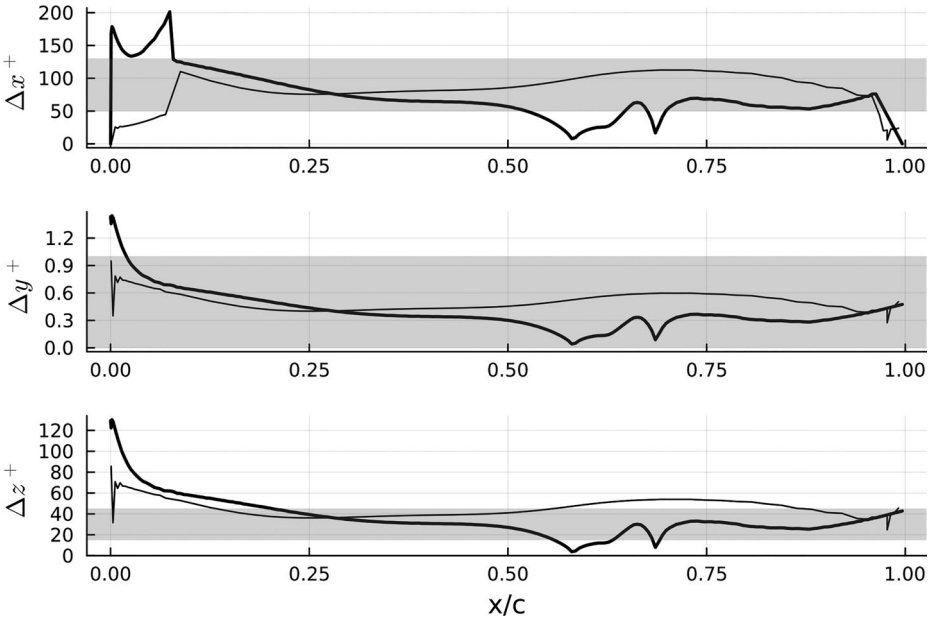

Fig. 3 Chordwise wall-refinement in the streamwise (Δx^+), normal (Δy^+) and spanwise (Δz^+) directions. DU89-134, Reynolds 500 000 AoA 5°, LS-VMS results are compared to Choi and Moin guidelines (Choi and Moin 2012) (gray area). The suction side data are highlighted by using a thicker line

Table 2 Mesh characteristics for les case of SD7003, E387, and DU89-134

Case	$\Delta y_0/c$ (wall-normal)	$\Delta x/c$ (curvilinear coordinates)	$\Delta z/c$
SD7003	1.5×10^{-4}	6.7×10^{-3}	9.1×10^{-3}
E387	2.5×10^{-5}	6.7×10^{-3}	-
DU89-134 ($\mathcal{M}$)	1.7×10^{-5}	5.0×10^{-3}	3.1×10^{-3}

Table 3 DU89-134, Reynolds 500 000 at 5° RANS convergence analysis

Mesh Setting	Coarse	Medium	Fine	Very Fine
Number of Cells	4.51×10^4	1.88×10^5	8.90×10^5	1.15×10^6
Number of Prism Layers	25	30	35	38
Divisions along the airfoil chord	50	100	200	225
Average y^+	0.46	0.57	0.27	0.25

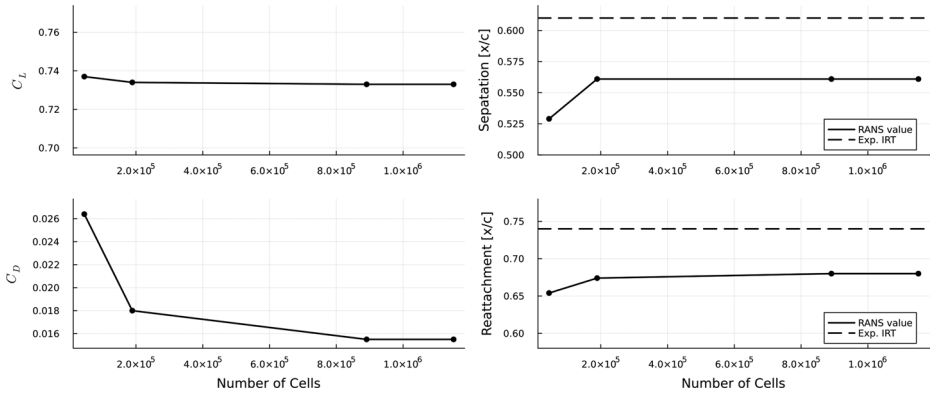

Fig. 4 RANS convergence analysis

$y^+ \leq 1$, as recommended by (Menter et al. 2015). The mesh convergence study for the case of the DU89-134, Reynolds 500 000 AoA 5° are presented in Table 3 and Fig. 4.

5 Results

5.1 SD7003 Validation

The SD7003 airfoil at Reynolds 60 000 and AoA 4° is one of the most popular airfoils for studying LSB and the capability of the numerical method of capturing it. In Fig. 5a, the C_f and C_p results obtained with the LS-VMS are compared with the LES proposed by (Galbraith et al. 2008), the two-scale VMS (Calderer and Masud 2013), DNS performed in (Wiart and Hillewaert 2012; Carreño Ruiz and D'Ambrosio 2022), PIV measurements (Ol et al. 2012; Tangermann et al. 2017), pressure taps and Oil Film Interferometry (OFI) (Sutton 2015). RANS simulations have been carried out using the Suluksna-Juntasaro calibration, (Suluksna et al. 2009) with the standard value s_1=6. As noted in (Carreño Ruiz

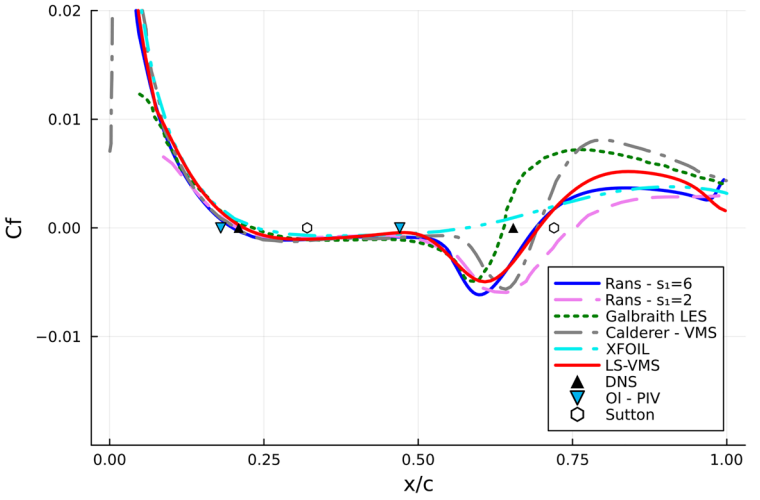

(a) SD7003 C_f results comparison. For DNS, PIV and Sutton, separation and reattachment point are plotted

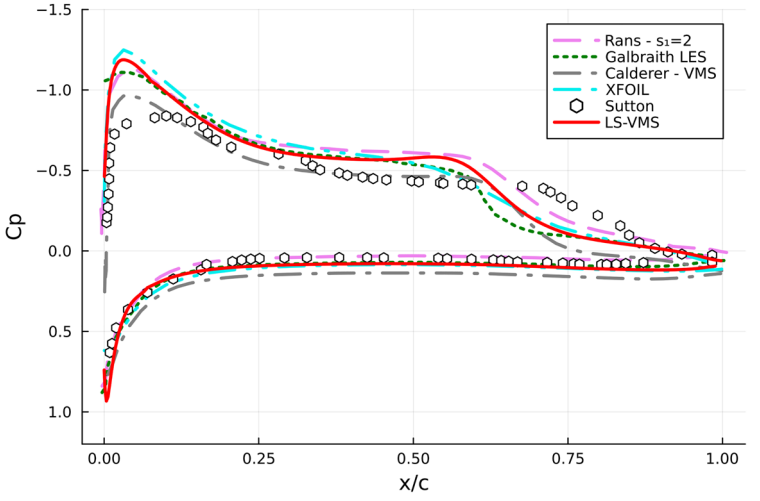

(b) SD7003 C_p results comparison

Fig. 5 Pressure and friction coefficients for SD7003 at Reynolds 60 000 and 4°

and D'Ambrosio 2022), the RANS solution strongly depends on the parameter s_1. It can be changed to move the reattachment point, Fig. 6a, so, also use the value $s_1=2$ is used, since it leads to a better prediction for this specific case.

All the numerical methods identify the separation point at the same location: $\frac{x_{sep}}{c} \approx 0.2$. Different experimental techniques, PIV (Ol et al. 2012), and OFI (Sutton 2015), locate it in two different positions, 4, where the PIV result is closer to the numerical results.

Table 4 Aerodynamic coefficients and LSB characteristics for different models, SD7003 Reynolds 60 000 and 4°

	$\frac{x_{sep}}{c}$	$\frac{x_{reatt}}{c}$	C_L	C_D
LS-VMS (present study)	0.23	0.690	0.601	0.0236
Suluksna-Juntasaro	0.184	0.743	0.600	0.0257
LES (Galbraith et al. 2008)	0.23	0.65	0.59	0.021
VMS (Calderer and Masud 2013)	0.222	0.665	-	-
DNS (Wiart and Hillewaert 2012)	0.209	0.654	0.602	0.0196
PIV (Tangermann et al. 2017)	0.286	0.783	-	-
PIV (Ol et al. 2012)	0.18	0.58	-	-
Experiments: pressure taps and OFI (Sutton 2015)	-	-	0.57	-

The main discrepancies arise in the location of the transition and reattachment point. Galbraith tends to predict reattachment too close to the leading edge, while VMS predicts reattachment closer to the trailing edge than DNS. It is reassuring that two independent VMS implementations derived from the VMS locate the reattachment precisely at the same spot. The differences are in the transition point and the bubble length.

Analyzing the overall aerodynamic performances C_L and C_D, Table 4 the differences between all the methods are limited, proving that the VMS can be used on transitional airfoils to predict aerodynamic performances. The C_L is calculated correctly and perfectly aligned with the DNS results. The C_D is overestimated compared to both LES and VMS. In conclusion, LS-VMS can detect the LSB on the suction on the airfoil and provide an estimation of the aerodynamic coefficients. The pressure distribution curves, Fig. 5b, are in general agreement with each other. The experimental values from pressure taps (Sutton 2015) reveal a less steep pressure decrease after the bubble reattaches, and numerical methods tend to predict a stronger suction peak in the proximity of the leading edge. It is important to note that discrepancies between experimental and computational results do not necessarily indicate that the measurements are inaccurate. Instead, obtaining reliable experimental data for this case is inherently challenging due to its strong dependence on the experimental setup. Similarly, computational results are highly sensitive to numerical and modeling choices, as evident from the observed variations. The overall sensitivity of the case leads to a significant spread in results, highlighting the difficulty of achieving consistent agreement between different approaches.

RANS models need to be calibrated using LES and DNS, or experiments where available, to obtain better results. For example, (Carreño Ruiz and D'Ambrosio 2022) showed how a value of $s_1 = 6$ causes the reattachment point to retract and be closer to the location predicted with the LES and VMS.

Lastly, the velocity profiles in vertical planes at different locations on the top side of the airfoil are extracted and compared with published results. Figure 6 shows the comparison between the velocity obtained with the LS-VMS and the wrLES published by (Schmidt and Breuer 2017), showing a very close agreement.

The profiles of the Reynolds stress tensor $(\overline{u'u'})/U_\infty^2$ are reported in Fig. 7 for $x/c = [0.40, 0.44, 0.48, 0.52, 0.56, 0.60]$. The results are compared with the WR-LES simulation of (Schmidt and Breuer 2017) as well as experimental measurements of (Windte et al. 2006) (WIW) and (Hain et al. 2009) (WAH). Overall, both the shape and magnitude of the profiles agree well. However, the LS-VMS tends to predict larger off-wall stress levels, which may reflect differences in the reference conditions. In particular, Hain 2009 report a

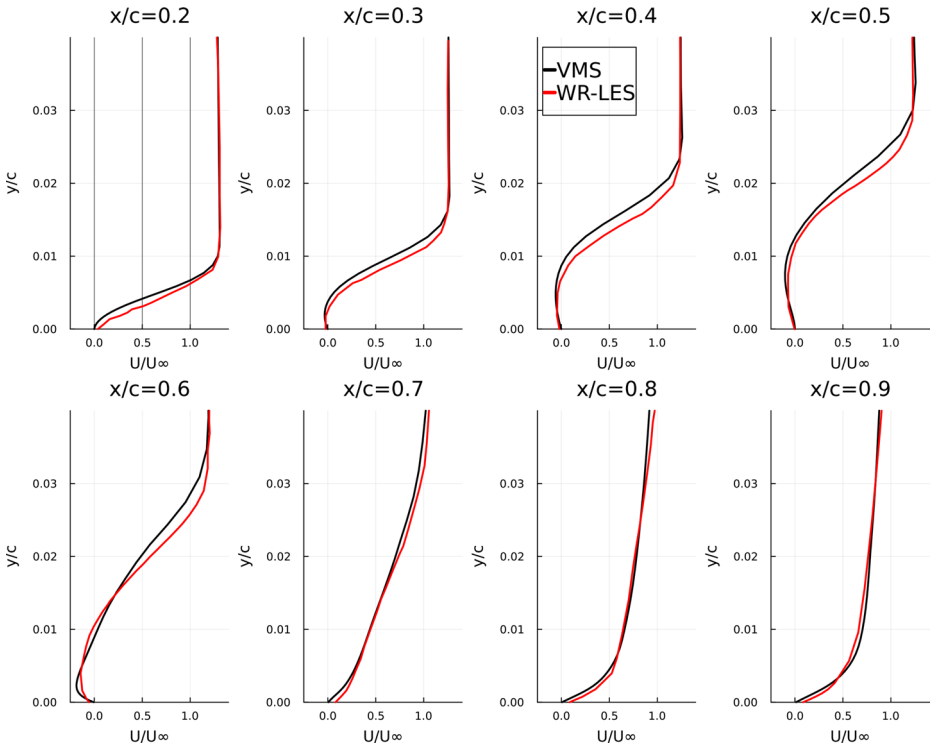

Fig. 6 SD7003 at Reynolds 60 000 and 4° velocity profiles compared to WR-LES results (Schmidt and Breuer 2017)

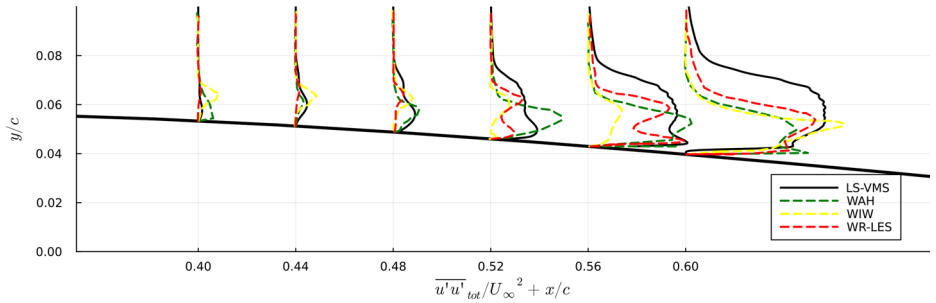

Fig. 7 SD7003 at Reynolds 60 000 and 4° total Reynolds stress, comparison with WR-LES simulation of (Schmidt and Breuer 2017), experimental measurements of (Windte et al. 2006) (WIW) and (Hain et al. 2009) (WAH)

higher Reynolds number ($Re = 66\,000$), and Schmidt 2017 employ an incoming turbulence intensity of $TI = 0.28\%$.

Figure 8a shows the iso-surfaces of the Q-criterion, which highlight the vortical structures forming in the separated shear layer over the suction side of the SD7003 airfoil. The roll-up of the shear layer into coherent vortices and their subsequent breakdown into smaller scales can be clearly identified, marking the transition from laminar to turbulent flow above

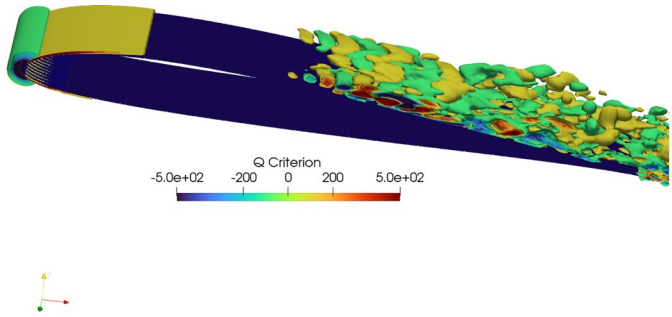

(a) SD7003 instantaneous iso-surfaces of Q- criterion

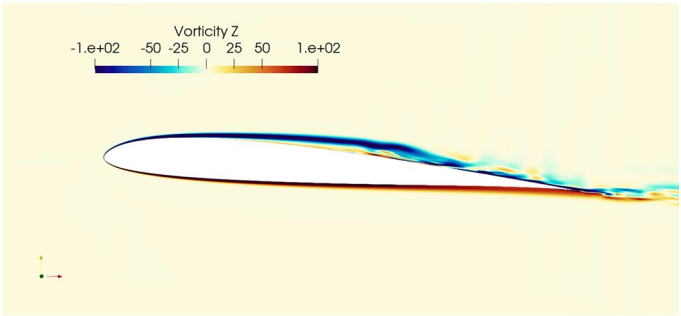

(b) SD7003 w_z

Fig. 8 Instantaneous Q-criterion iso-surfaces and w_z display for SD7003 at Reynolds 60 000 and 4°

the LSB. Extremely similar structures have been published by (Uranga et al. 2011; Calderer and Masud 2013; Galbraith et al. 2008). Figure 8b presents the instantaneous spanwise vorticity field ω_z, similarly as in (Uranga et al. 2011; Galbraith et al. 2008). The separated shear layer is visible as a region of concentrated vorticity just above the suction surface, with alternating bands indicating the presence of Kelvin–Helmholtz instabilities. Downstream of reattachment, the vorticity field becomes increasingly irregular, confirming the development of a turbulent boundary layer. Together, the Q-criterion and ω_z visualizations provide qualitative evidence of the transition process across the LSB.

5.2 E387 Validation

The Eppler 387 airfoil coordinates have been taken from (McGhee et al. 1988) and this airfoil has been chosen as further validation due to its well-documented LSB. The simulations are performed at Reynolds number 3×10^5 and $AoA = 1°$ as in (Carreño Ruiz and D'Ambrosio 2022; Catalano and De Rosa 2020). The time-averaged C_p distribution is compared with experimental results from (McGhee et al. 1988), and it assess further the ability of iLES to predict the formation of the LSB, Fig. 9. Both 2D and 3D simulations are conducted. The final time-step solution of the 2D simulation has been used to initialize the 3D simulation. The 3D computation is initialized by extruding the converged 2D solution in the spanwise direction. No artificial 3D perturbation is added: the initial spanwise velocity component is set to zero. After a short initial transient, during which the intrinsic instability of

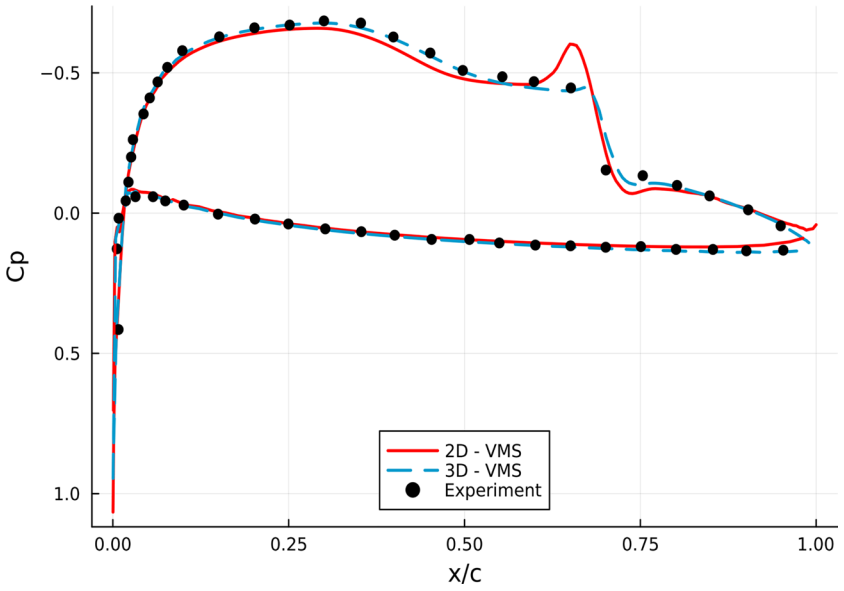

Fig. 9 Time averaged C_p on the E387 airfoil at Reynolds number 3×10^5 and $AoA = 1^\circ$ 2D and 3D simulations. Comparison with experimental results from (McGhee et al. 1988)

the separated shear layer grow, the flow becomes fully three-dimensional. This transient is discarded when collecting statistics. Both for 2D and 3D simulations the time-step adopted is $\Delta t = 0.001$ Figure 1.5 shows a generally good agreement in the C_p distribution between the 2D and 3D simulations. However, notable differences arise due to the absence of spanwise effects in the 2D simulations. It is well established that 2D unsteady NS simulations are often considered inadequate, as the spanwise component plays a crucial role in flow development. In the case of the LSB, the primary differences between 2D and 3D simulations could derive from the influence of spanwise flow structures, which affect transition and reattachment mechanisms. A key feature in the 2D C_p distribution is the plateau followed by a localized pressure suction peak at $x/c \approx 0.7$. This peak is a characteristic artifact of purely 2D simulations, as previously observed in (Koning et al. 2023), and is attributed to the lack of spanwise breakdown of vortical structures. Without the third dimension, the vertical structures in 2D have no means to diffuse into 3D structures, resulting in prolonged vortex convection compared to the 3D case. By contrast, the 3D simulation captures a smoother transition, with the characteristic pressure plateau followed by a more gradual drop, which is an indication of the development of an LSB. The ability of the 3D simulation to correctly predict this feature highlights the importance of resolving spanwise instabilities in capturing the true physics of transitional flows. These differences further emphasize the limitations of purely 2D approaches for flows involving separation, transition, and reattachment.

5.3 DU89-134

This research aims to use VMS to investigate the performance of high L/D ratio airfoil, testing specifically the DU89-134 (Boermans and Garrel 1997). The testing conditions are at

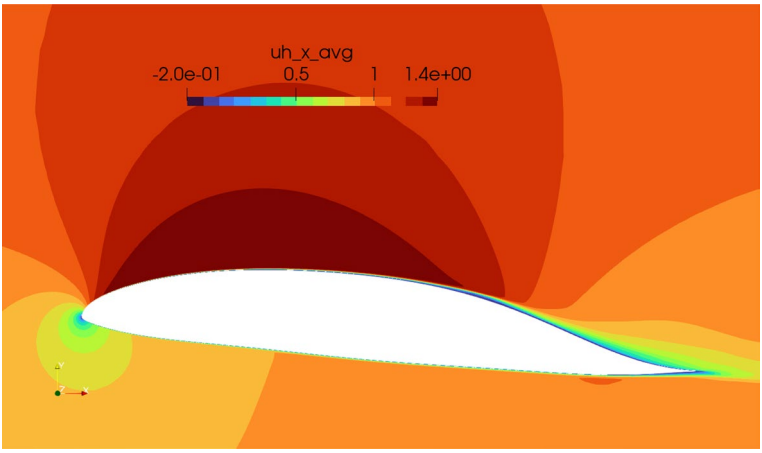

Fig. 10 DU89-134 at $Re = 500\,000$, AoA 5° time-averaged velocity field

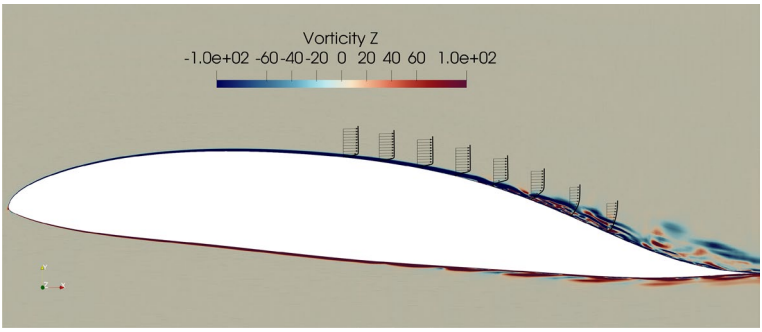

Fig. 11 DU89-134 at $Re = 500\,000$, AoA 5° instantaneous spanwise vorticity and average velocity profiles

$Re = 500\,000$ at $AoA = 1°, 5°$. Figure 10 shows the average velocity field and the detail of the recirculating bubble on the suction side, and Fig. 11 shows the instantaneous spanwise vorticity and average velocity profiles.

5.3.1 C_L, C_D, Separation, and Reattachment

As can be seen in Figs. 12 and 13, the average pressure and shear stress distributions obtained with the LS-VMS are compared to those obtained with RANS coupled with the transitional model using the Suluksna-Juntasaro correlation (Suluksna et al. 2009), the RANS results obtained with ANSYS in (Avirovic et al. 2023), XFOIL simulations. In Fig. 12 are also marked the separation and reattachment point detected experimentally using InfraRed Thermography (IRT) (Avirovic et al. 2024). Experiments are carried out in the Royal Military Academy open-circuit low-speed and low-turbulence wind tunnel. More details about the wind tunnel facility can be found in (Avirovic et al. 2023). Table 5 presents a comparison of

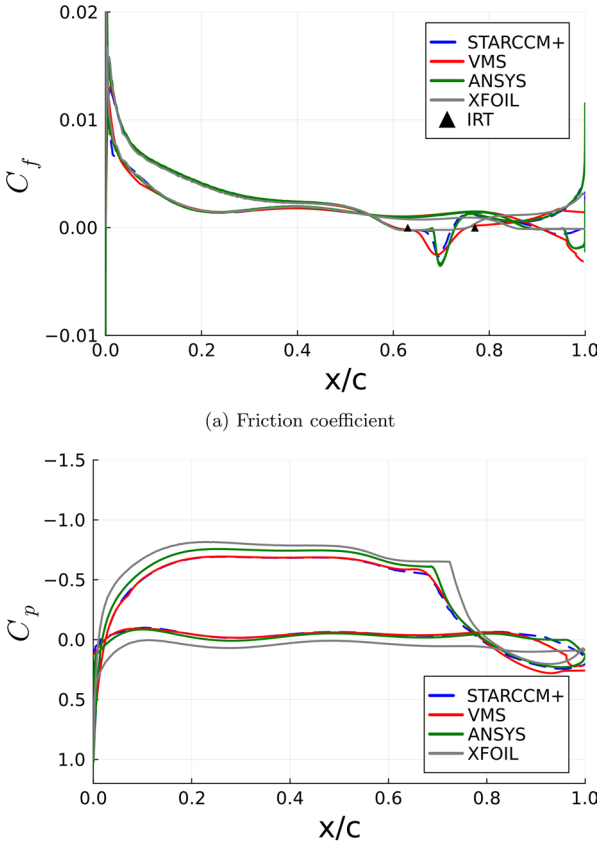

(a) Friction coefficient

(b) Pressure coefficient

Fig. 12 DU89-134, Reynolds 500 000 AoA 1°, STARCCM+ and VMS

C_L, C_D, and the locations of separation and reattachment points at angles of attack 1° and 5°, for all the aforementioned numerical and experimental methods.

Both at 1° and 5°, XFOIL fails in predicting separation and reattachment. While the XFOIL solution shows a slightly negative skin–friction coefficient on the upper surface, the values remain extremely small (of order 10^{-4}) and nearly flat. Such behaviour does not represent a resolved separation bubble: XFOIL does not predict a meaningful separation or reattachment point for this case. This is a direct consequence of its formulation: XFOIL couples a linear-vorticity panel method with an integral boundary-layer solver and an e^N transition criterion, and is therefore limited to a two-dimensional viscous–inviscid interaction framework (Drela 1989). While it has proven effective for rapid analysis and design of low Reynolds number airfoils (Drela 1988), it cannot capture the inherently three-dimensional mechanisms involved in the breakdown of a LSB, such as spanwise instabilities, vortex roll-up, and secondary flows. These processes strongly influence transition onset and reattachment, and their absence in XFOIL often leads to discrepancies with experimental measurements or high-fidelity CFD simulations (Gunel et al. 2016; Morgado et al. 2016).

An additional aspect to consider is the choice of the transition amplification factor n_{crit}, which directly relates to the free-stream turbulence intensity of the environment where the airfoil is tested. In XFOIL, n_{crit} effectively sets the receptivity of the boundary layer to

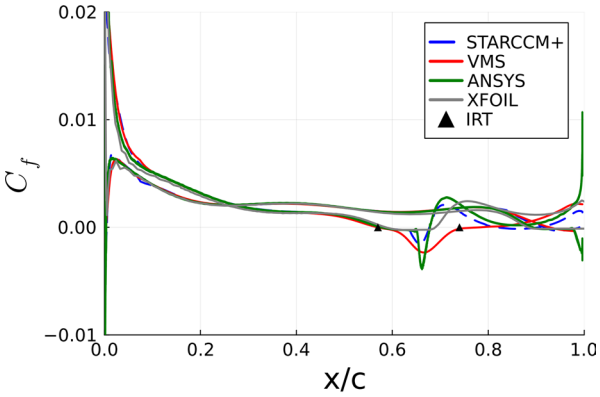

(a) Friction coefficient

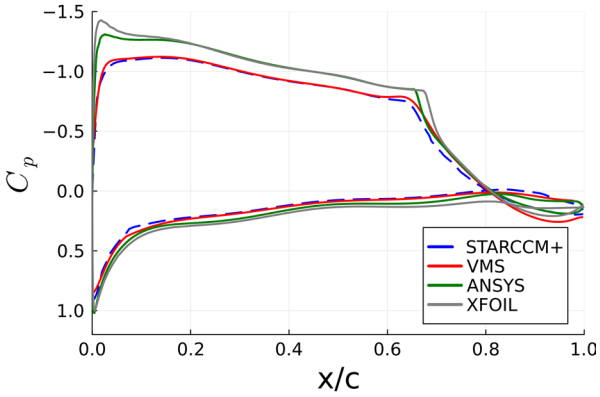

(b) Pressure coefficient

Fig. 13 DU89-134, Reynolds 500 000 AoA 5°, STARCCM+ and VMS

Table 5 DU89-134, Reynolds 500 000 VMS and RANS results

	AoA [°]	$\frac{x_{sep}}{c}$	$\frac{x_{reatt}}{c}$	C_L	C_D
XFOIL	1	-	-	0.34	0.0119
RANS (STARCCM+)	1	0.60	0.72	0.342	0.0102
RANS (Avirovic et al. 2023)	1	0.60	0.72	0.41	0.0108
VMS	1	0.60	0.76	0.351	0.0095
Experimental (Avirovic et al. 2024)	1	0.63	0.77	-	-
XFOIL	5	-	-	0.992	0.00959
RANS (STARCCM+)	5	0.58	0.67	0.776	0.0146
RANS (Avirovic et al. 2023)	5	0.55	0.69	0.79	0.013
VMS	5	0.57	0.80	0.789	0.0127
Experimental (Avirovic et al. 2024)	5	0.61	0.74	-	-

external disturbances. Using the relation presented in (Van Ingen 2008), $n_{\text{crit}} = 10$ corresponds to a turbulence intensity of approximately 0.11%, which is close to the value of wind tunnel facility used for experiments. Therefore, the selection of n_{crit} is fundamental to ensure consistency between numerical predictions and experimental conditions. The XFOIL computations were carried out using 400 surface panels, with additional refinement applied

along the upper surface. For the DU89-134 airfoil, LS-VMS is proven to be capable of predicting the LSB on the suction side of the airfoil. Separation points location do not appear to vary significantly with different methods. In general, its locations vary with respect to the IRT results by less than 5%. In the specific case of DU89-134, the main differences arise after the transition point. RANS anticipates the location of the reattachment compared to VMS and experiments, leading to a shorter LSB. This effect translates into a higher C_D. For the 5° case, RANS predicts a reattachment followed by another separation. Using the Suluksna-Juntasaro correlation method and not modifying the RANS parameters in the $\gamma - Re\theta$ model the reattachment point could be shifted downstream, as in the SD7003, or upstream, in this case. The derivative $\frac{dC_f}{dx}$ at reattachment location is higher in RANS than in LS-VMS for both cases. For 1° the LS-VMS is predicting reattachment within 1% error compared with IRT experiments. For the 5° the reattachment point for LS-VMS is delayed by 6% in the LS-VMS prediction in comparison with the IRT location. The main explanation can be that, as mentioned before, the $\frac{dC_f}{dx}$ is approaching zero between $0.75c - 0.85c$.

In consideration of the cases seen and viewed, numerical methods (VMS, RANS, LES) do not encounter specific difficulties in predicting the separation point, for all the cases there is always a substantial agreement. The main difference between the methods is in the identification of the reattachment location.

RANS models struggle fundamentally with LSBs due to their closure assumptions and empirical basis. Even transition-sensitive RANS formulations, such as the γ–Re_θ model, rely on empirical correlations for the transition onset and length based on flat-plate or attached boundary-layer data (Langtry et al. 2006). When applied to separated transitional flows, these correlations can become unreliable, often leading to inaccurate predictions of bubble length, reattachment location, and pressure recovery (Celik et al. 2008). By construction, therefore, RANS are not able to always resolve accurately the underlying instability mechanisms. This motivates the use of higher-fidelity approaches such as LES or LS-VMS, which explicitly resolve the shear-layer instabilities and their nonlinear breakdown into turbulence.

5.3.2 Velocity Profiles and Hot-Wires Anemometry

The velocities in the *x* direction along vertical planes at different locations on the upper side of the airfoil are extracted, time and span averaged, and compared with the experimental results obtained with the hot-wire anemometry technique.

The results in Fig. 14 show close agreement between the experimental and the numerical data. However, in practice, with hot-wire anemometry, it is challenging to have the first measuring point exactly attached to the wall, especially in the transitional/turbulent region. Furthermore, the hot wire is an intrusive technique, which alters the flow, and this can be a reason of the minor discrepancies with the LES results. Despite these challenges, the strong agreement between the LES and experimental profiles outside the near-wall region reinforces the accuracy and reliability of the numerical method in capturing key flow characteristics. The ability of LES to resolve the near-wall dynamics without experimental intrusiveness further highlights its advantage in studying complex boundary layer phenomena.

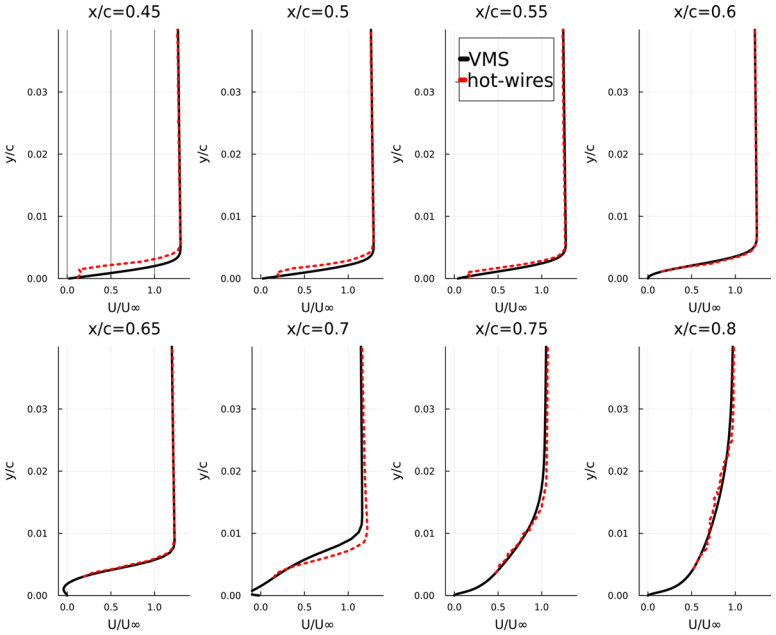

(a) DU89-134, Reynolds 500 000 1°

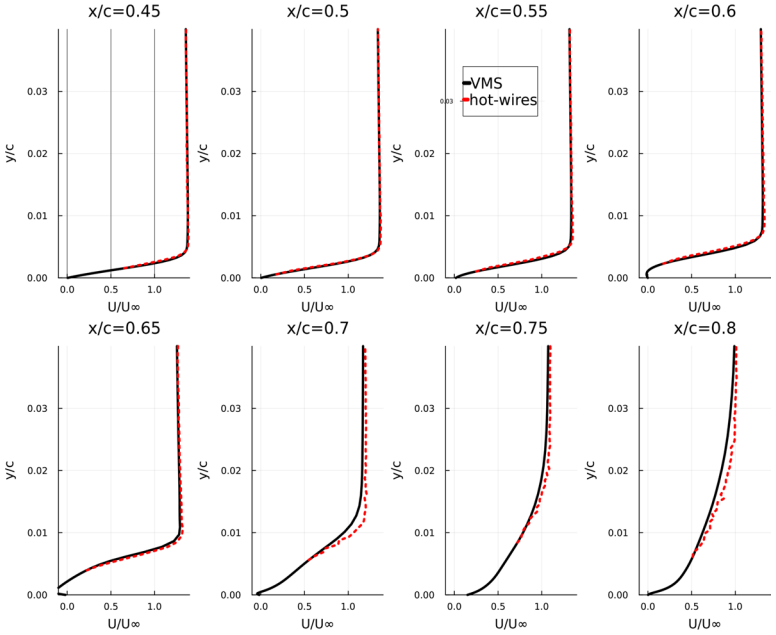

(b) DU89-134, Reynolds 500 000 5°

Fig. 14 Comparison of the velocity profiles at several chordwise positions on the suction side between the present VMS and hot-wire measurement

5.3.3 Kinetic Energy Spectra

The turbulent kinetic energy spectra in Figs. 15 and 16 are obtained at different chord-length locations. For each, the analysis is performed by collecting data at multiple points aligned along the spanwise direction (z-axis) and averaging these measurements to obtain representative energy spectra. Four distinct spectra are reported for the 2 configurations of the DU89-134 airfoil. The spectrum at $x/c = 0.6$ has a turbulent kinetic energy of 6 order of magnitude less than the others, clearly indicating laminar flow.

The spectra at $x/c = [0.7, 0.8, 0.9]$ are computed at $y^+ \approx 220$. They do not yet display a fully developed $-5/3$ inertial subrange; however, the broadening of energy towards higher frequencies and the steepening of the decay are clear indicators of a flow undergoing transi-

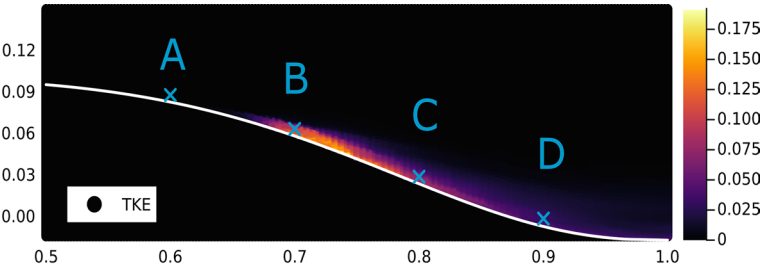

(a) Turbulent kinetic energy on the suction side of the airfoil and spectra locations

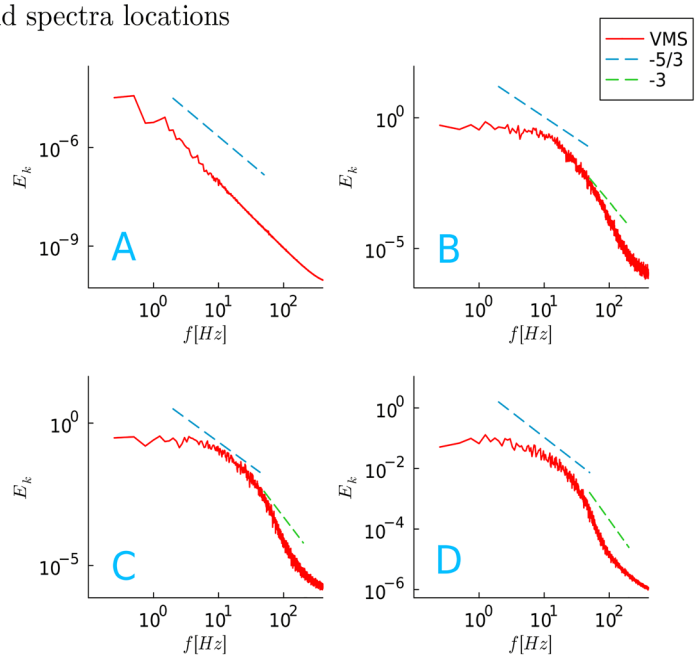

(b) TKE spectra

Fig. 15 DU89-134, Reynolds 500 0001° kinetic energy spectra. The spectrum serves as a diagnostic of flow state and numerical dissipation; the $-5/3$ slope is shown as a reference. (**a**) Turbulent kinetic energy on the suction side of the airfoil and spectra locations. (**b**) TKE spectra

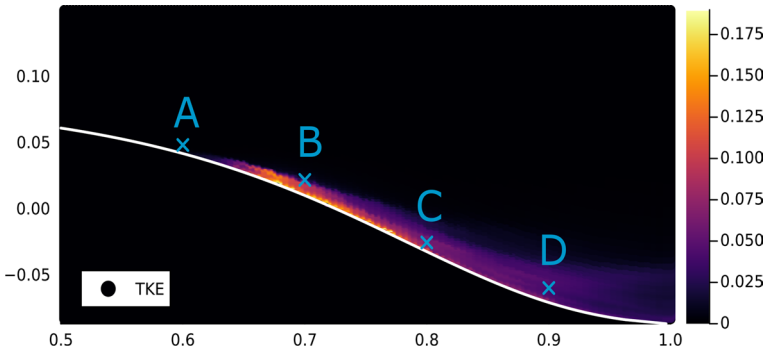

(a) Turbulent kinetic energy on the suction side of the airfoil and spectra locations

(b) TKE spectra

Fig. 16 DU89-134, Reynolds 500 0005° kinetic energy spectra. The spectrum serves as a diagnostic of flow state and numerical dissipation; the $-5/3$ slope is shown as a reference

tion. Our intent is to use the spectra primarily to discriminate between laminar and turbulent regions across the LSB. Similarly to the observations of (Garmann et al. 2013), a limited $-5/3$ trend can be identified downstream of reattachment, whereas upstream, in the laminar portion of the flow, no such scaling appears. The spanwise averaging of the measurements enhances the statistical reliability of the results and provides a robust validation of the numerical approach.

6 Mesh and Time Sensitivity

Mesh and time sensitivity have been performed for $Re = 500000\, AoA = 1°, 5°$. A slight dependence of C_L and C_D on mesh resolution and time step is observed, but the overall trends remain consistent, suggesting that the solution is nearly grid- and time-converged. Figure 17 reports the Q-criterion isosurfaces for different mesh resolution.

6.1 Mesh Independence Study

$\mathcal{M}$ - medium, $\mathcal{C}$ - coarse, $\mathcal{F}$ - fine, $\mathcal{SF}$ - super fine - meshes have been tested, Table 6. Mesh sensitivity analysis has been studied for the case Reynolds number $500\,000$, AoA 1°. In all cases, the condition $y^+ < 1$ over the airfoil is ensured.

6.2 Time Independence Study

The same case used for mesh independence has been used for studying the dependence of the results on the time step using the $\mathcal{M}$ mesh. At higher Reynolds numbers, the char-

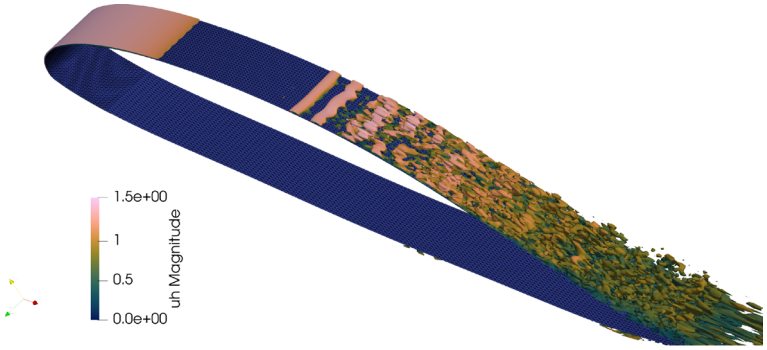

(a) Q-criterion isosurface for mesh $\mathcal{C}$

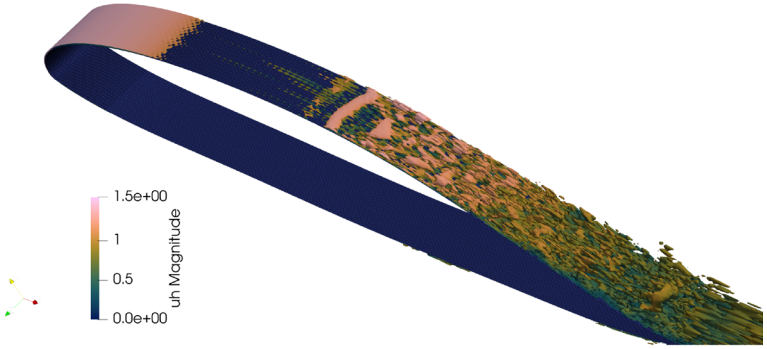

(b) Q-criterion isosurface for mesh $\mathcal{F}$

Fig. 17 DU89-134, Reynolds $500\,000\, 5°$ Q-criterion isosurface for $Q = 500$ for different meshes

Table 6 Mesh sensitivity analysis DU89, Reynolds 500 000, AoA 1°

Mesh settings	$\mathcal{C}$	$\mathcal{M}$	$\mathcal{F}$	$\mathcal{SF}$
Airfoil divisions	150	200	200	300
Z divisions	12	16	22	16
First cell height [m]	4.8e-6	2.8e-6	1.6e-6	1.6e-6
CL	0.3539	0.3514	0.3504	0.3519
CD	0.00915	0.00950	0.00929	0.00947
Separation $[x/c]$	0.60	0.60	0.60	0.60
Reattachment $[x/c]$	0.77	0.76	0.76	0.75

Table 7 Time sensitivity analysis DU89, Reynolds 500 000, AoA 1°

dt$[s]$	2.0×10^{-3}	1.0×10^{-3}	5.0×10^{-4}
CL	diverged	0.3514	0.3511
CD	diverged	0.00950	0.00911
Separation $[x/c]$	diverged	0.60	0.60
Reattachment $[x/c]$	diverged	0.76	0.73

Table 8 Time average sensitivity analysis DU89, Reynolds 500 000, AoA 1°

	$\mathcal{C}$	$\mathcal{C}$	$\mathcal{M}$	$\mathcal{M}$
ftt	10	20	10	20
C_L	0.3538	0.3539	0.3516	0.3514
C_D	0.00910	0.00915	0.00939	0.00950
Separation $[x/c]$	0.60	0.60	0.60	0.60

acteristic time scale reduces, so it is worth testing it. Results are shown in Table 7 where $\Delta t > 1\ 10^{-3}$ simulations are diverging.

Although time integration is implicit, practical stability and accuracy constraints still apply due to the finite element spatial discretization and flow physics. Classical von Neumann stability analysis holds only in idealized cases (linear PDEs, uniform grids, periodic boundaries) and does not extend to realistic finite element schemes and unsteady nonlinear flows. Moreover, stability remains closely tied to dimensionless parameters such as the Courant and the local Péclet number. For example, (Bazilevs et al. 2007) uses a very small time-step, of the order of 0.2 the adective Courant number.

It is likely due to a violation of the CFL, even though iLES employs an implicit time-stepping, which relaxes the strict CFL constraint that explicit schemes have, the numerical stability is still affected when Δt is too large.

It is also investigated whether the time interval of $10 ftt$ is enough to obtain convergent results, Table 8. Aerodynamic coefficients and the separation point location converge quickly, as the results are also averaged in the spanwise direction.

The sensitivity analysis shows that as the mesh is refined, C_D varies by approximately 2–3%, while C_L and the separation point location remain largely unchanged.

7 Conclusion

This study investigated the feasibility and accuracy of predicting the development of LSB on airfoils at low-Reynolds-number using the LS-VMS, in comparison with traditional approaches (RANS). The numerical method was validated against experimental data for well-known airfoils, specifically the SD7003 and E387, demonstrating its capability to accurately predict the LSB creation and transition phenomena and highlight the limits of simple and fast 2D approaches.

The main novelty of this study was focusing on the DU89-134 airfoil, which is of interest for HAPS applications. The numerical results, compared with experiments, confirm that the VMS method effectively predicts the separation and reattachment locations, aerodynamic coefficients, and boundary layer characteristics, strengthening its applicability for airfoil analysis in this context. The spectral analysis of the turbulent kinetic energy shows an approximate $-5/3$ trend over a limited range of frequencies after the reattachment point, in agreement with earlier investigations (Garmann et al. 2013). While not indicative of a fully developed inertial subrange, this behaviour is consistent with the expected dynamics of the transitional shear layer and lends confidence to the robustness of the method. Additionally, the mesh and time sensitivity analysis revealed that the aerodynamic coefficients and separation point location remain largely stable under refinement, with C_D varying within 2–3%. These findings suggest that the linearized VMS method provides an efficient and accurate alternative to traditional methods for studying low-Reynolds-number airfoils.

As a future direction, the adjoint method could be integrated into the framework to enable aerodynamic shape optimization, improving the design of airfoils for HAPS applications. Additionally, extending the approach to fully three-dimensional simulations and investigating its performance under freestream turbulence conditions would further enhance its applicability.

Acknowledgements The corresponding author gratefully acknowledges Prof. Georg May for his valuable support and insightful discussions during the initial phase of this work.

Author Contributions C. B. wrote the main manuscript and prepared all the figures. All authors reviewed the manuscript.

Funding This research has been financed by the Royal Higher Institute for Defense for funding this research through the project MSP21/02 Numerical and Experimental Low Speed High Altitude Wing (NELSHAW).

Data Availability No datasets were generated or analysed during the current study.

Declarations

Competing Interests The authors declare no competing interests.

References

Ahmed, N., Chacón Rebollo, T., John, V., Rubino, S.: A review of variational multiscale methods for the simulation of turbulent incompressible flows. Archiv. Comput. Methods Eng. **24**(1), 115–164 (2017). https://doi.org/10.1007/s11831-015-9161-0

Avirovic, M., Brunelli, C., Marinus, B.G., Degroote, J., Van Beeck, J.: Numerical and experimental study of laminar-turbulent transition on a laminar airfoil at low Reynolds number. In: AIAA Aviation Forum. American Institute of Aeronautics and Astronautics (2023). https://doi.org/10.2514/6.2023-3674

Avirovic, M., Brunelli, C., Marinus, B.G., Degroote, J., Van Beeck, J.: Laminar-turbulent transition on a DU89-134 airfoil at low Reynolds number for use at high altitude. In: AIAA Aviation Forum and Ascend. American Institute of Aeronautics and Astronautics, Las Vegas, Nevada (2024). https://doi.org/10.2514/6.2024-3998

Bazilevs, Y., Calo, V.M., Cottrell, J.A., Hughes, T.J.R., Reali, A., Scovazzi, G.: Variational multiscale residual-based turbulence modeling for large eddy simulation of incompressible flows. Comput. Methods Appl. Mech. Eng. **197**, 173–201 (2007). https://doi.org/10.1016/j.cma.2007.07.016

Beck, A.D., Bolemann, T., Flad, D., Frank, H., Gassner, G.J., Hindenlang, F., Munz, C.: High-order discontinuous Galerkin spectral element methods for transitional and turbulent flow simulations. Int. J. Numer. Methods Fluids **76**, 522–548 (2014). https://doi.org/10.1002/fld.3943

Boermans, L.M., Garrel, A.V.: Design and windtunnel test results of a flapped laminar flow airfoil for high-performance sailplane applications (1997)

Brooks, A.N., Hughes, T.J.R.: Streamline upwind/Petrov-Galerkin formulations for convection dominated flows with particular emphasis on the incompressible Navier-Stokes equations. Comput. Methods Appl. Mech. Eng. **32**, 199–259 (1982). https://doi.org/10.1016/0045-7825(82)90071-8

Brunelli, C.: SegregatedVMSSolver.Jl: linearized and Segregated stabilized solver for large eddy simulation in Julia. J. Open Source Softw. **10**(110), 7564 (2025). https://doi.org/10.21105/joss.07564

Brunelli, C., Avirovic, M., Janssens, B., Marinus, B.G., May, G., Runacres, M.: Prediction of a laminar separation bubble on low-Reynolds airfoils using variational multiscale method. In: AIAA Aviation Forum Ascend. American Institute of Aeronautics and Astronautics (2024). https://doi.org/10.2514/6.2024-4261

Brunelli, C., Avirovic, M., Janssens, B., Marinus, B.G., Runacres, M.: Numerical and experimental study of effects of triangular cross-Section riblets on DU89-134 airfoil. Aerotec. Missili & Spazio (2025). https://doi.org/10.1007/s42496-025-00258-4

Brunelli, C., Avirovic, M., Janssens, B., Marinus, B.G., Runacres, M., May, G., Ecorce, A., Dalbera, A.: Passive flow control devices on low-Reynolds DU89-134 airfoil. In: 34th Congress of the International Council of the Aeronautical Sciences (2024)

Calderer, R., Masud, A.: Residual-based variational multiscale turbulence models for unstructured tetrahedral meshes. Comput. Methods Appl. Mech. Eng. **254**, 238–253 (2013). https://doi.org/10.1016/j.cma.2012.09.015

Carreño Ruiz, M., D'Ambrosio, D.: Validation of the $\gamma - Re_\theta$ transition model for airfoils operating in the very low Reynolds number regime. Flow, Turbul. Combust. **109**, 279–308 (2022). https://doi.org/10.1007/s10494-022-00331-z

Catalano, P., De Rosa, D.: Large eddy simulations and RANS models for airfoils at low Reynolds number. In: AIAA Aviation Forum. American Institute of Aeronautics and Astronautics (2020). https://doi.org/10.2514/6.2020-2990

Celik, I.B., Ghia, U., Roache, P.J., Freitas, C.J., Coleman, H., Raad, P.E.: Procedure for estimation and reporting of uncertainty due to discretization in CFD applications. J. Fluids Eng., Trans. ASME **130**(7), 0780011–0780014 (2008). https://doi.org/10.1115/1.2960953

Choi, H., Moin, P.: Grid-point requirements for large eddy simulation: Chapman's estimates revisited. Phys. Fluids **24**(1), 011702 (2012). https://doi.org/10.1063/1.3676783

Drela, M.: Low-Reynolds-number airfoil design for the M.I.T. Daedalus prototype- a case study. J. Aircr. **25**(8), 724–732 (1988). https://doi.org/10.2514/3.45650

Drela, M.: XFOIL: an analysis and design system for low Reynolds number airfoils in Low Reynolds Number Aerodynamics, T.J. Mueller (ed.), vol. 54, pp. 1–12. Springer (1989). https://doi.org/10.1007/978-3-642-84010-4_1

Evans, J.A., Kamensky, D., Bazilevs, Y.: Variational multiscale modeling with discretely divergence-free subscales. Comput. Math. Appl. **80**(11), 2517–2537 (2020). https://doi.org/10.1016/j.camwa.2020.03.011

Franca, L.P., Hughes, T.J.R.: Two classes of mixed finite element methods. Comput. Methods Appl. Mech. Eng. **69**(1), 89–129 (1988). https://doi.org/10.1016/0045-7825(88)90168-5

Frère, A., Hillewaert, K., Chatelain, P., Winckelmans, G.: High Reynolds number airfoil: from wall-resolved to wall-modeled les. Flow, Turbul. Combust. **101**(2), 457–476 (2018). https://doi.org/10.1007/s10494-018-9972-9

Galbraith, M.C., Visbal, M.R., Student, G.: Implicit large eddy simulation of low Reynolds number flow past the SD7003 airfoil. In: 16th AIAA Aerospace Sciences Meeting and Exhibit (2008). https://doi.org/10.2514/6.2008-225

García-Gutiérrez, A., Gonzalo, J., Domínguez, D., López, D., Escapa, A.: Aerodynamic optimization of propellers for high altitude Pseudo-Satellites. Aerosp. Sci. Technol. **96** (2020). https://doi.org/10.1016/j.ast.2019.105562

Garmann, D.J., Visbal, M.R., Orkwis, P.D.: Comparative study of implicit and subgrid-scale model large-eddy simulation techniques for low-Reynolds number airfoil applications. Int. J. Numer. Methods Fluids **71**, 1546–1565 (2013). https://doi.org/10.1002/fld.3725

Geuzaine, C., Remacle, J.-F.: Gmsh: a three-dimensional nite element mesh generator with built-in pre- and post-processing facilities. Int. J. Numer. Methods Eng. (2009). https://doi.org/10.1002/nme.2579

Gunel, O., Koc, E., Yavuz, T.: CFD vs. XFOIL of airfoil analysis at low reynolds numbers. IEEE. (2016). https://doi.org/10.1109/ICRERA.2016.7884411

Hain, R., Kähler, C.J., Radespiel, R.: Dynamics of laminar separation bubbles at low-Reynolds-number aerofoils. J. Fluid Mech. **630**, 129–153 (2009). https://doi.org/10.1017/S0022112009006661

Hosseini, S.M., Vinuesa, R., Schlatter, P., Hanifi, A., Henningson, D.S.: Direct numerical simulation of the flow around a wing section at moderate reynolds number. Int. J. Heat Fluid Flow. **61**, 117–128 (2016). https://doi.org/10.1016/j.ijheatfluidflow.2016.02.001

Hughes, T.J.R.: Multiscale phenomena: Green's functions, the dirichlet-to-neumann formulation, subgrid scale models, bubbles and the origins of stabilized methods. Comput. Methods Appl. Mech. Engrg **127**, 387–401 (1995). https://doi.org/10.1016/0045-7825(95)00844-9

Hughes, T.J.R., Feijóo, G.R., Mazzei, L., Quincy, J.-B.: The variational multiscale method—a paradigm for computational mechanics. Comput. Methods Appl. Mech. Eng. **166**, 3–24 (1998). https://doi.org/10.1016/S0045-7825(98)00079-6

Hughes, T.J.R., Franca, L.P., Balestra, M.: A New finite element formulation for computational fluid dynamics: V. Circumventing the Babuška-Brezzi condition: a stable Petrov-Galerkin formulation of the Stokes problem accommodating equal-order interpolations. Comput. Methods Appl. Mech. Eng. **59**(1), 85–99 (1986). https://doi.org/10.1016/0045-7825(86)90025-3

Hughes, T.J.R., Mazzei, L., Jansen, K.E.: Large eddy simulation and the variational multiscale method. Comput. Visual Sci. **3**, 47–59 (2000). https://doi.org/10.1007/s007910050051

Janssens, B.: Numerical modeling and experimental investigation of fine particle coagulation and dispersion in dilute flows. PhD thesis, Von Karman Institute for Fluid Dynamics, Université de la Rochelle -UFR science et technologie, Royal Military Academy (2014)

John, V.: Finite element methods for incompressible flow problems. In: Springer Series in Computational Mathematics, vol. 51. Springer, Berlin, Germany (2016). https://doi.org/10.1007/978-3-319-45750-5

Kenji Takizawa, S.M.D.M., Tezduyar, T.E.: Space-time VMS methods for modeling of incompressible flows at high reynolds numbers. Math. Model Methods Appl. Sci. **23**, 223–248 (2013). https://doi.org/10.1142/S0218202513400022

Koning, W.J.F., Romander, E.A., Cummings, H.V., Perez Perez, B.N., Buning, P.G.: On improved understanding of airfoil performance evaluation methods at low Reynolds numbers. J. Aircr. **60**(3), 774–788. (2023) https://doi.org/10.2514/1.C037023

Langtry, R.B., Menter, F.R., Likki, S.R., Suzen, Y.B., Huang, P.G., Völker, S.: A correlation-based transition model using local variables - part ii: test cases and industrial applications. J. Turbomach. **128**, 423–434 (2006). https://doi.org/10.1115/1.2184353

Lee, D., Nonomura, T., Oyama, A., Fujii, K.: Comparative studies of numerical methods for evaluating aerodynamic characteristics of two-dimensional airfoil at low Reynolds numbers. Int. J. Comput. Fluid Dyn. **31**, 57–67 (2017). https://doi.org/10.1080/10618562.2016.1274398

McGhee, R.J., Walker, B.S., Millard: B.F.: Experimental results for the Eppler 387 airfoil at low Reynolds numbers in the Langley low-turbulence pressure tunnel (1988)

Menter, F.R., Smirnov, P.E., Liu, T., Avancha, R.: A one-equation local correlation-based transition model. Flow. Turbul. Combust. **95**, 583–619 (2015). https://doi.org/10.1007/s10494-015-9622-4

Morgado, J., Vizinho, R., Silvestre, M.A.R., Páscoa, J.C.: XFOIL vs CFD performance predictions for high lift low Reynolds number airfoils. Aerosp. Sci. Technol. **52**, 207–214 (2016). https://doi.org/10.1016/j.ast.2016.02.031

Mourousias, N., García-Gutiérrez, A., Malim, A., Fernández, D.D., Marinus, B.G., Runacres, M.C.: Uncertainty quantification study of the aerodynamic performance of high-altitude propellers. Aerosp. Sci. Technol. **133** (2023). https://doi.org/10.1016/j.ast.2023.108108

Ol, M., McCauliffe, B., Hanff, E., Scholz, U., Kaehler, C.: Comparison of laminar separation bubble measurementson a low Reynolds number airfoil in three facilities. In: 35th AIAA Fluid Dynamics Conference and Exhibit, American Institute of Aeronautics and Astronautics. (2012) https://doi.org/10.2514/6.2005-5149

Piomelli, U.: Wall-layer models for large-eddy simulations. Prog. Aerosp. Sci. **44**(6), 437–446 (2008). https://doi.org/10.1016/j.paerosci.2008.06.001

Rasthofer, U., Gravemeier, V.: Recent developments in variational multiscale methods for large-eddy simulation of turbulent flow. Archiv. Comput. Methods Eng. **25**(3), 647–690 (2018). https://doi.org/10.1007/s11831-017-9209-4

Sagaut, P.: Large Eddy simulation for incompressible flows: an introduction, 3rd edn. Springer, Berlin, Germany (2006)

Schlichting, H., Gersten, K.: Boundary-Layer theory. Springer, Berlin (2016). https://doi.org/10.1007/978-3-662-52919-5

Schmidt, S., Breuer, M.: Source term based synthetic turbulence inflow generator for eddy-resolving predictions of an airfoil flow including a laminar separation bubble. Comput. Fluids. **146**, 1–22 (2017). https://doi.org/10.1016/j.compfluid.2016.12.023

Schmidt, S., Franke, M., Thiele, F.: Assessment of SGS models in les applied to a NACA 4412 airfoil. In: 39th Aerospace Sciences Meeting and Exhibit. American Institute of Aeronautics and Astronautics (2012). https://doi.org/10.2514/6.2001-434

Selig, M.S., Donovan, J.F., Fraser, D.B.: Airfoils at low speeds. H.A. Stokely, Virginia Beach (1989)

Suluksna, K., Dechaumphai, P., Juntasaro, E.: Correlations for modeling transitional boundary layers under influences of freestream turbulence and pressure gradient. Int. J. Heat Fluid Flow. **30**(1), 66–75 (2009). https://doi.org/10.1016/j.ijheatfluidflow.2008.09.004

Sutton, D.M.: Experimental characterization of the effects of freestream turbulence intensity on the SD7003 airfoil at low Reynolds numbers. (2015)

Tangermann, E., Klein, M., Herbst, S.L., Hain, R., K, C.J.: Numerical and experimental investigation of the flow around a three-dimensional SD7003 wing. In: 10th International Symposium on Turbulence and Shear Flow Phenomena (2017)

Trofimova, A.V., Tejada-Martínez, A.E., Jansen, K.E., Lahey, R.T.: Direct numerical simulation of turbulent channel flows using a stabilized finite element method. Comput. Fluids **38**, 924–938 (2009). https://doi.org/10.1016/j.compfluid.2008.10.003

Uranga, A., Persson, P.O., Drela, M., Peraire, J.: Implicit large eddy simulation of transition to turbulence at low Reynolds numbers using a discontinuous Galerkin method. Int. J. Numer. Methods Eng. **87**, 232–261 (2011). https://doi.org/10.1002/nme.3036

Van Ingen, J.: The e^N method for transition prediction. Historical review of work at tu Delft. In: 38th Fluid Dynamics Conference and Exhibit, American Institute of Aeronautics and Astronautics, Seattle, Washington (2008). https://doi.org/10.2514/6.2008-3830

Wiart, C.C.D., Hillewaert, K.: DNS and ILES of transitional flows around a SD7003 using a high order discontinuous Galerkin method. In: Seventh International Conference on Computational Fluid Dynamics (ICCFD7), Big Island, Hawaii (2012, July, 9–13)

Windte, J., Scholz, U., Radespiel, R.: Validation of the RANS-simulation of laminar separation bubbles on airfoils. Aerosp. Sci. Technol. **10**, 484–494 (2006). https://doi.org/10.1016/j.ast.2006.03.008

Authors and Affiliations

Carlo Brunelli[1,2,3] · Matija Avirovic[1,3,4] · Bart Janssens[1] · Benoît G. Marinus[1] · Koen Hillewaert[3,5] · Mark Runacres[2]

✉ Carlo Brunelli
carlo.brunelli@mil.be

Matija Avirovic
matija.avirovic@mil.be

Bart Janssens
bart.janssens@mil.be

Benoît G. Marinus
benoit.marinus@mil.be

Koen Hillewaert
koen.hillewaert@uliege.be

Mark Runacres
mark.runacres@vub.be

[1] MECA, Royal Military Academy, Renaissancelaan 30, Brussels 1000, Belgium

[2] Engineering Technology, Vrije Universiteit Brussel, Pleinlaan 2, Brussels 1050, Belgium

[3] Aeronautics and Aerospace, von Karman Institute for Fluid Dynamics, Waterloosesteenweg 72, Sint-Genesius-Rode B-1640, Belgium

[4] Faculty of Engineering and Architecure, Department of ElectroMechanical, Systems and Metal Engineering, Ghent University, Sint-Pietersnieuwstraat, Gent 9000, Belgium

[5] University of Liège, Liège, Belgium